Exceptional points in rolled-up tubular microcavities

2017 J. Opt. 19 095101

(http://iopscience.iop.org/2040-8986/19/9/095101)

IOP Publishing Journal of Optics
J. Opt. 19 (2017) 095101 (7pp) https://doi.org/10.1088/2040-8986/aa7796

Exceptional points in rolled-up tubular microcavities

Yangfu Fang[1], Shilong Li[2,4], Suwit Kiravittaya[3] and Yongfeng Mei[1,4]

[1] Department of Materials Science, Fudan University, 220 Handan Road, Shanghai 200433, People's Republic of China
[2] National Laboratory for Infrared Physics, Shanghai Institute of Technical Physics, Chinese Academy of Sciences, 500 Yutian Road, Shanghai 200083, People's Republic of China
[3] Department of Electrical and Computer Engineering, Faculty of Engineering, Naresuan University, Taphoo, Muang, Phitsanulok 65000, Thailand

E-mail: shilong@mail.sitp.ac.cn and yfm@fudan.edu.cn

Received 12 May 2017
Accepted for publication 6 June 2017
Published 24 July 2017

Abstract

We observe the crossing and anti-crossing behaviors of nearly degenerate mode pairs in a rolled-up tubular microcavity, which can be explained by weak and strong couplings between the modes. Exceptional points (EPs) are thus obtained in the tubular microcavity since they are the critical point where a transition from strong to weak coupling occurs. Rolled-up tubular microcavities with a given resonant mode approaching an EP in parameter space expanded by two continuous variables are also realized without using near-field probes. Microcavities with EPs prepared in a rolled-up way could be mechanically stable and would be used for optofluidic detection.

Keywords: exceptional points, rolled-up microcavities, chaotic microcavities

(Some figures may appear in colour only in the online journal)

1. Introduction

Exceptional points (EPs) are singularities in parameter space, at which eigenvectors and eigenvalues of a non-Hermitian system coalesce [1–4]. These eigenvalue surfaces present a complex-square-root topology around a branch point at the EP. The topological structure of EPs is nontrivial and leads to richer and broader physics, ranging from the Berry phase [5, 6] and quantum chaos [7] to non-reciprocity of light in a parity-time related system [8, 9]. Recently, the optical detection of single particles using EPs in microcavities has been proposed, and a sevenfold enhanced sensitivity compared to that when using diabolic points (DPs) has been proved based on an analytical theory and numerical simulations [10–12]. The anomalous enhancement of sensitivity also results from the nontrivial topology of EPs, which gives rise to an energy splitting proportional to $\sqrt{\epsilon}$ when an EP is subjected to a perturbation of strength ϵ. The same perturbation strength ϵ on a DP leads to an energy splitting proportional to ϵ. Therefore, the splitting of energy induced by a given weak perturbation ($\epsilon < 1$) using EPs is larger than that using DPs so that an enhanced sensitivity is achieved. This finding benefits not only the development of high-sensitivity optical detection, but also the promotion of physics related to EPs.

To this end, microcavities with a well-defined EP are desired. The originally proposed microcavity for EPs is a two-particle microdisk system [10], as shown in figure 1(a). The size of the two particles and their distance to the microdisk are adjusted to drive eigenvalues of this microcavity system to EPs. The two-particle microdisk structure is motivated by recent experiments on a microtoroid microcavity subjected to two near-field nanofiber probes [13, 14]. Obviously, a precise position control of the near-field probes is mandatory for this implementation. However, it might suffer from the unavoidable mechanical vibration of the *external* long and thin nanofibers. As a result, a variation of the two-particle microdisk system has been introduced where EPs are prepared by two small holes inside the microdisk [11]. Nevertheless, microcavities that have EPs are few and limited to the

[4] Authors to whom any correspondence should be addressed.

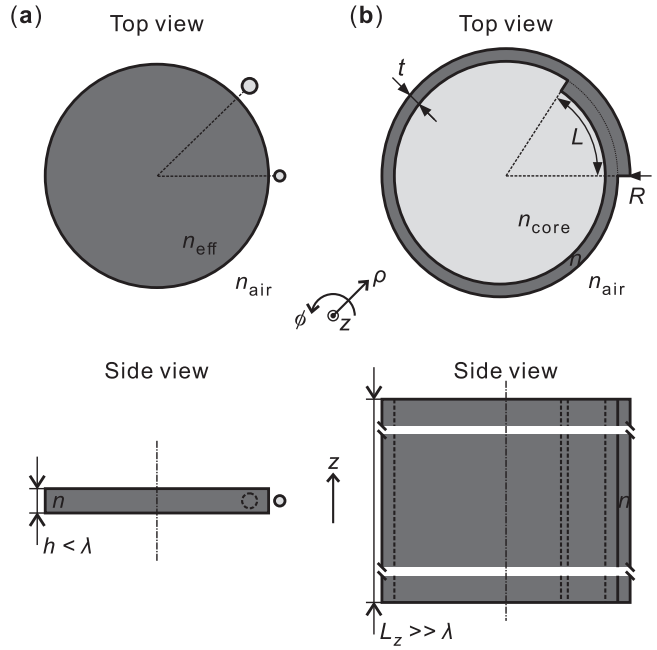

Figure 1. Comparison between a two-particle microdisk system and a rolled-up tubular microcavity. (a) The two-particle microdisk system consists of a microdisk microcavity subjected to two near-field particles. EPs are obtained by varying the size of the *external* near-field particles and their distance to the microdisk microcavity. The thickness h of the microdisk is generally smaller than the vacuum wavelength λ in order to apply the effective index approximation. (b) The rolled-up tubular microcavity is formed by releasing a strained nanomembrane. The ends of the nanomembrane become notches of the tubular microcavity. The *internally* generated notches play the role of near-field particles for the microcavity to drive it to EPs. The length L_z of the rolled-up tubular microcavity is set to be much larger than the vacuum wavelength λ, so that it can be considered as an infinitely long cylinder. Other parameters are defined in the main text.

microdisk system, and heavily rely on *external* near-field probes.

In this paper, we realize EPs in rolled-up tubular microcavities without using any *external* near-field probes. The structure of a rolled-up tubular microcavity is formed by rolling up a nanomembrane with certain curvatures [15], as shown in figure 1(b). As can be seen, the structural notches in the microcavity play the role of two particles or holes in the microdisk system, but are *internally* formed during the rolling process [15]. As demonstrated later, EPs emerge in the rolled-up tubular microcavity by merely varying the distance between notches, which implies that this microcavity system with EPs could be mechanically stable. In addition, EPs in rolled-up tubular microcavities could be used for optofluidic detection due to their integrability in the microfluidic channel structure [16]. Optofluidic detection in rolled-up tubular microcavities has been demonstrated in a well-controlled manner [16–18]. Therefore, these findings would add functionality to optical detection using EPs as well as a deeper understanding of physics and applications in rolled-up tubular microcavities.

The remainder of this paper is organized as follows. Section 2 defines rolled-up tubular microcavities and numerical results on EPs are presented in section 3. Remarks on experimental realization of EPs in rolled-up tubular microcavities are given in section 4. We summarize our results in section 5.

2. Rolled-up tubular microcavities

Rolled-up tubular microcavities have, in the last decade, been widely investigated, from fabrication and characterization to optical detection [15–25], owing to the customizability of their geometry and material. In this paper, we consider the rolled-up tubular microcavity with a continuous translational symmetry along the axial z direction (see figure 1(b)). It can be fulfilled by using the same rolling length along the axial direction and setting the axial length L_z to a very large value compared to the vacuum wavelength λ. In addition, only homogeneous isotropic non-magnetic dielectric materials are taken into account. Therefore, Maxwell's equations can be reduced to a three-dimensional scalar Helmholtz equation, in the cylindrical coordinate system (ρ, ϕ, z),

$$\nabla^2\psi + \frac{\omega^2}{c^2}n^2(\rho, \phi, z)\psi = 0, \tag{1}$$

where ψ is the wave function, ω is the complex frequency, c is the speed of light in vacuum, and $n(\rho, \phi, z)$ is the piecewise constant refractive index. Due to the subwavelength-thin wall thickness normally used in rolled-up tubular microcavities, resonance modes with a transverse magnetic (TM) polarization preferably exist and are considered in this paper. For TM modes, the electric field vector $\boldsymbol{E}(\rho, \phi, z, t) \propto (0, 0, Re[\psi(\rho, \phi, z)e^{-i\omega t}])$ has only a non-zero z component. Moreover, the rolled-up tubular microcavity is translationally invariant in the axial z direction, one can thus separate the lateral field $\Theta(\rho, \phi)$ from the axial field $\Psi(z) \propto e^{ik_z z}$

$$\psi(\rho, \phi, z) \propto \Theta(\rho, \phi)e^{ik_z z}, \tag{2}$$

where k_z is a conserved quantity.

The continuous changing of k_z turns all discrete resonances into bands [26], which can possibly overlap (i.e. possible degeneracy between different resonant modes for specific non-zero k_z). The presence of the bands and the resultant degeneracies would significantly affect the properties of EPs. To avoid such bands and degeneracies, we fix k_z to be close to 0 in this paper. Fortunately, $k_z \approx 0$ is just the case for rolled-up tubular microcavities. In experiments, the spectrum of a rolled-up tubular microcavity is obtained either by micro-photoluminescence (μ-PL) spectroscopy where the emitted PL light is collected by the microscope objective perpendicular to the microcavitys z-axis [19], or by a near-field fiber where the transmitted light is guided perpendicular to the microcavity's z-axis [27]. In both situations, k_z is about 0. Now, the wave function $\psi \propto \Theta(\rho, \phi)$ is governed by the two-dimensional lateral Helmholtz equation

$$\left[\nabla_\perp^2 + \frac{\omega^2}{c^2}n^2(\rho, \phi)\right]\psi = 0. \tag{3}$$

However, as seen in figure 1(b), the lack of rotational symmetry in the lateral cross section makes the wave system non-integrable so that the finite element method (FEM) is used to solve this two-dimensional differential equation with Sommerfeld radiation wave conditions at infinity [28, 29].

The boundary of rolled-up tubular microcavities as shown in figure 1(b) is defined as

$$\rho(\phi) = R\left(1 - \frac{t}{2\pi}\phi\right), \tag{4}$$

where R is the outermost radius at $\phi = 0$ and t is the thickness of a single nanomembrane layer. The outer boundary jumps back to R at $\phi = 2\pi$ forming the outer notch, while the inner notch emerges at $\phi = L/R_{\text{avg}}$. Here, the overlap length L is determined by the rolling length and R_{avg} is the average radius of the rolled-up structure.

Although we make certain simplifications in this paper, the customizability of rolled-up tubular microcavities in their geometry and material has not been discounted. For example, the structural adjustability (R, t, and especially L) is still obvious, and the material (and thus the refractive indices n and n_{core}) can be arbitrary. Moreover, it is important to emphasise that $n(\rho, \phi)$ in equation (3) is not an effective one as generally presented in microdisk microcavities [30], so that it has less wavelength dependency which further ensures the stability and reliability of parameters for pursuing EPs in rolled-up tubular microcavities.

3. Exceptional points in rolled-up tubular microcavities

In order to observe EPs, a two-dimensional parameter space has to be constructed to visualize them. Owing to the customizability of rolled-up tubular microcavities, one can, in principle, arbitrarily select two of their structural and material parameters. Throughout this paper, however, only one structural parameter, i.e. the overlap length L, is used because it can be easily determined in experiments by specifying the rolling length before release. Another parameter used in this paper is from the material, i.e. the refractive index n_{core}, which can also be easily specified in experiments by controlling the component or concentration of solution inside the tubular core of the rolled-up structure after the rolling. As for other quantities, such as the thickness $t = 100\,\text{nm}$, the refractive indices $n = 2.0$, $n_{\text{air}} = 1.0$ and the outermost radius $R = 5\ \mu\text{m}$ are kept as constants, and the refractive index $n_{\text{core}} = 1.0$ is used unless otherwise noted.

Resonant wavelengths and the corresponding quality (Q) factors for two typical resonant modes (indicated by the azimuthal mode indices $m = 96$ and $m = 103$) in the rolled-up tubular microcavity are shown in figure 2. As can be seen, there is a nearly degenerate pair of modes for each given azimuthal mode index m, and crossing or anti-crossing behavior of resonant wavelengths and Q factors of the degenerated modes is clearly visible as the overlap length L varies. Moreover, there is a transition for the crossing and anti-crossing behaviors between the two resonant modes, i.e. the crossing (anti-crossing) behavior of resonant wavelengths (Q factors) for $m = 96$ (figure 2(a)) and the opposite behavior for $m = 103$ (figure 2(b)).

For microcavities with a rotational symmetry, there is a degenerate pair of modes for a given azimuthal mode index m. According to the position representation, the degenerate modes are named as clockwise (CW) and counterclockwise (CCW) propagating modes, respectively [30]. As a result of the lack of rotational symmetry, the degeneracy of mode pairs in rolled-up tubular microcavities is broken, as shown in figure 2. It is called mode splitting and has been observed in recent experiments [31], and several theoretical studies on mode splitting have been reported [31–34]. However, none of these papers have been aware of the crossing and anti-crossing behaviors of mode splitting, or realized EPs with the help of mode splitting. The aim of this paper is to present a theoretical study which reveals that EPs are the mechanism behind the crossing and anti-crossing behaviors of mode splitting, and thus could be observed by monitoring mode splitting in rolled-up tubular microcavities.

In order to have a deeper understanding of the crossing and anti-crossing behaviors of nearly degenerate pairs of modes in rolled-up tubular microcavities, a simple model of a two-level open system with an effective coupling [6, 30, 34, 35] is introduced here. The corresponding non-Hermitian Hamiltonian reads

$$H = \begin{pmatrix} \omega_0 & 0 \\ 0 & \omega_0 \end{pmatrix} + \begin{pmatrix} \Gamma & A \\ B & \Gamma \end{pmatrix}. \tag{5}$$

Here eigenvectors of the first matrix correspond to the CCW and CW propagating modes with an equal frequency ω_0 without any coupling between them, whereas the second matrix takes the coupling into account. The diagonal elements of the second matrix stand for the total scattering rates Γ, while the off-diagonal elements describe the backscattering from the CW to CCW propagating mode (A) and from the CCW to CW propagating mode (B). By a direct diagonalization of the non-Hermitian Hamiltonian (5), eigenvalues and (not normalized) eigenvectors are obtained as

$$\omega_{\pm} = \omega_0 + \Gamma \pm \sqrt{AB}, \tag{6}$$

$$\psi_{\pm} = \begin{pmatrix} \sqrt{A} \\ \pm\sqrt{B} \end{pmatrix}. \tag{7}$$

It is necessary to note that the resonant wavelength is proportional to the real part of eigenvalues while the Q factor is inversely proportional to their imaginary part [7, 30]. Since A and B are independent complex numbers, $\sqrt{AB}$ can be an imaginary, a real, or a complex number. When $\sqrt{AB}$ is an imaginary number, the rolled-up tubular microcavity is in a weak coupling regime where a crossing occurs in resonant wavelengths of the CCW and CW propagating modes, as shown in the upper panel of figure 2(a). When $\sqrt{AB}$ is a real number, the rolled-up tubular microcavity is in a strong coupling regime where a crossing occurs in Q factors of the CCW and CW propagating modes, as shown in the lower panel of figure 2(b). It is noted that around the region of crossing in both the weak and strong regimes, the eigenstates

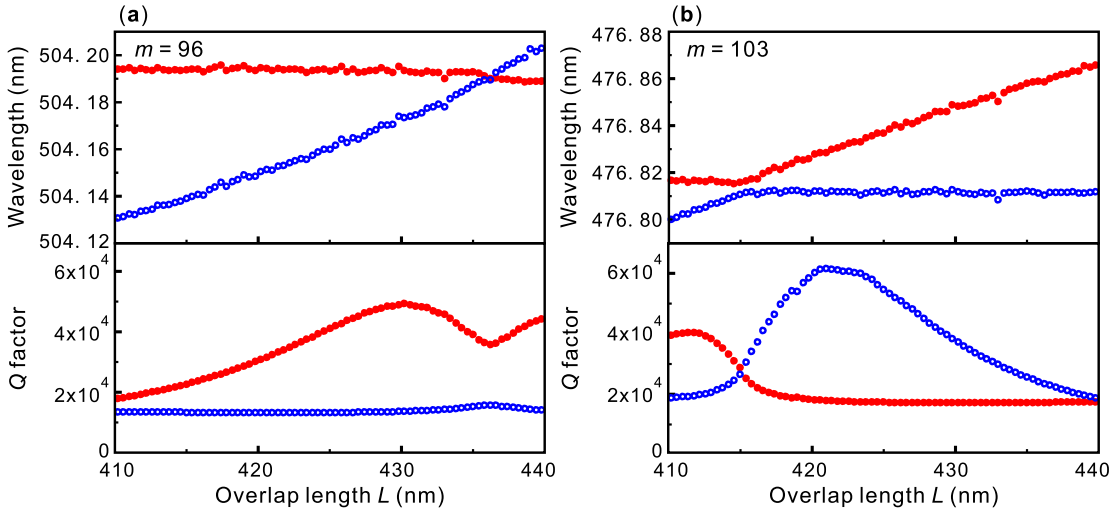

Figure 2. Crossing and anti-crossing behaviors for nearly degenerate mode pairs (red solid and blue hollow circles) as the overlap length L varies. (a) Crossing of resonant wavelengths (the upper panel) while anti-crossing of the corresponding Q factors (the lower panel) for resonant mode $m = 96$. (b) Anti-crossing of resonant wavelengths (the upper panel) while crossing of the corresponding Q factors (the lower panel) for resonant mode $m = 103$. Small deviations from the smoothly varied data points are due to the finite size of structural meshes used for FEM simulations.

are hybridized, i.e. the eigenvectors of the non-Hermitian Hamiltonian (5) are superpositions of eigenvectors of the first matrix (i.e. the effective uncoupled Hamiltonian). Additionally, the hybridization is weak in the weak coupling regime. For the special case $A = 0$ or $B = 0$, both resonant wavelengths and Q factors of the CCW and CW propagating modes cross

$$\omega_{\pm} = \omega_0 + \Gamma. \tag{8}$$

Simultaneously, the eigenvectors collapse to a single one

$$\psi_{\pm} = \begin{pmatrix} 0 \\ 1 \end{pmatrix} \text{ or } \begin{pmatrix} 1 \\ 0 \end{pmatrix}. \tag{9}$$

In such a case, an EP is obtained.

As described by the simple model, crossing and anti-crossing behaviors of nearly degenerate pairs of modes in rolled-up tubular microcavities originate from coupling between them, which can be weak or strong. Actually, EPs are the critical point where a transition from strong to weak coupling occurs [7]. Therefore, it is better to seek EPs by looking for the transition between weak and strong couplings instead of searching the simultaneous crossing of resonant wavelength and Q factor. With this strategy, we find EPs in rolled-up tubular microcavities. Figure 3 shows the resonant wavelength and Q factor surfaces in m-L parameter space, both of which reveal the nontrivial complex-square-root topology around a branch point, indeed, at an EP. Such an EP in parameter space expanded by the azimuthal mode index m has been experimentally observed in a deformed microdisk microcavity [36] where they called m the 'internal parameter'. From this point of view, by taking the 'internal parameter' m into account, EPs are realized in rolled-up tubular microcavities by simply varying one structural parameter, i.e. the overlap length L.

It is noteworthy that the two-level non-Hermitian Hamiltonian model with an effective coupling used above might be oversimplified for considering the dissipative effects in our microcavity, which is an open quantum system. A strict theoretical treatment could be made based on a more general theory [37]. However, it is out of the scope of this paper.

For the sake of optical detection using EPs, it is better to push a single resonant mode m approaching an EP in the parameter space expanded by two continuous variables instead of the discrete 'internal parameter' m. To this end, the second continuous variable is required, which, as mentioned above, is from material, i.e. the refractive index n_{core}. Figure 4(a) shows the resonant wavelength surfaces in L-n_{core}^2 parameter space for resonant mode $m = 103$. As can be seen, an EP is clearly visible. As expected, it is the critical point where the transition between strong and weak couplings takes place, and is located at the branch point singularity of resonant wavelength surfaces with a complex-square-root topology. Further confirmation of the EP can be made by checking the non-orthogonality or (spatial) chirality of the nearly degenerate mode pair in the region close to the EP [30]. Figure 4(b) shows electric fields of the nearly degenerate pair of modes near the EP in the rolled-up tubular microcavity (the left panel), together with a degenerate mode pair in a ring microcavity with the same thickness t, average radius R_{avg} and mode indices as well as an equivalent resonant wavelength for comparison (the right panel). A closer look on these electric fields reveals that: (i) the degenerate mode pair for the ring microcavity has well-defined nodal lines at which the electric field intensity vanishes, while the nearly degenerate mode pair near the EP for the microcavity has less visibility of nodal lines which is the signature of (spatial) chirality due to an asymmetric transition between the CW and CCW components; (ii) the degenerate mode pair for the ring microcavity has an obvious orthogonality where a $\pi/2$ phase difference between its electric fields exists, while the nearly degenerate mode pair near the EP for the microcavity has an obscure orthogonality which is the signature of non-orthogonality

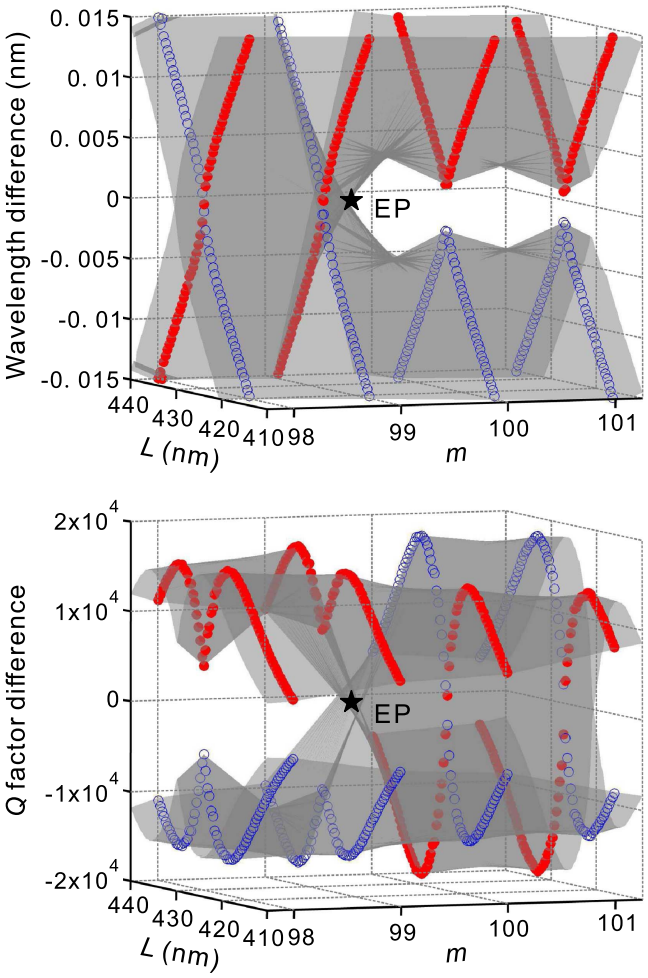

Figure 3. EP in *m*-*L* parameter space. Both the resonant wavelength (the upper panel) and *Q* factor (the lower panel) surfaces of nearly degenerate mode pairs (red solid and blue hollow circles) in *m*-*L* parameter space show a complex-square-root topology with a branch point singularity at the EP. To have a better view of the topology, these surfaces are constructed by the difference value between absolute and average values.

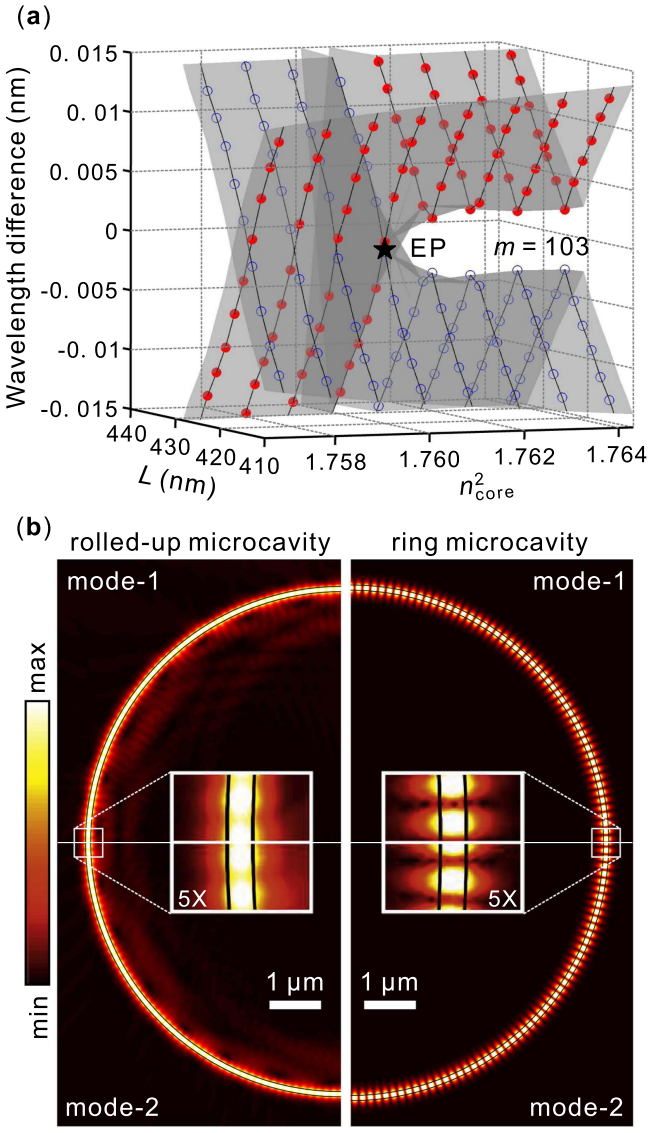

Figure 4. EP in L-n^2_{core} parameter space for resonant mode $m = 103$. (a) EP is the singular branch point of resonant wavelength surfaces with a complex-square-root topology. Red solid and blue hollow circles indicate the nearly degenerate mode pairs. To have a better view of the topology, these surfaces are constructed by the difference value between absolute and average values. (b) Electric field intensity $|\psi|^2$ of the nearly degenerate mode pair in the region close to the EP for the rolled-up tubular microcavity (the left panel consisted of two quarters of a complete rolled-up structure), and of the degenerate mode pair for the ring microcavity with the same thickness t, average radius R_{avg} and mode indices as well as an equivalent resonant wavelength (the right panel consisted of two quarters of a complete ring structure). Some discontinuities are visible in the enlarged view, and are due to the finite size of structural meshes used for FEM simulations.

because of the nearly identical electric fields. These observations confirm the finding of EP in rolled-up tubular microcavities.

4. Remarks on experimental realization of EPs in rolled-up tubular microcavities

Compared with the most extensively studied microdisk microcavities, there are a few particularities for the experimental realization of EPs in rolled-up tubular microcavities. First of all, rolled-up tubular microcavities generally have a subwavelength-thin wall thickness. This results in fully guided optical modes bound by both the inner and outer walls, which is not the case for other bulky microcavities. As we have found in our recent work [34], these fully guided optical modes in the subwavelength-thin-walled rolled-up tubular microcavities have a deterministic mode chirality due to strong resonant interactions between the inner and outer notches via scattered waves within the overlap area. Such strong resonant interaction has never been considered for bulky microdisk microcavities. As a result, the resonant modes in rolled-up microcavities are more sensitive to structural variation, and thus are more easily tuned to approach EPs. Secondly, as we have mentioned above, rolled-up tubular microcavities are vertically aligned and have a hollow core, which is in contrast to the in-plane solid

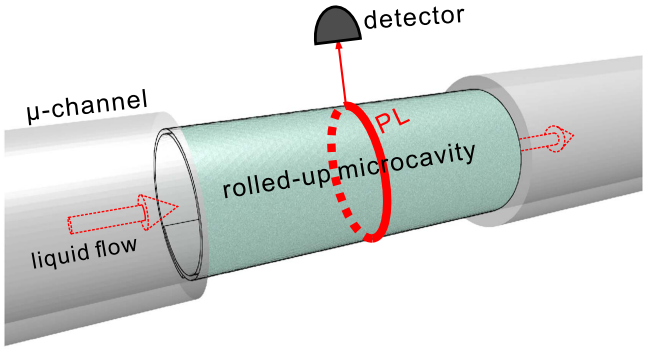

Figure 5. Integration of a rolled-up tubular microcavity with μ-channels for both the experimental realization of EPs and the label-free optofluidic detection using them. The spectral information of the rolled-up tubular microcavity is obtained by a μ-PL spectroscopy where the emitted PL light is collected by the microscope objective perpendicular to the microcavity's axis.

microdisk microcavities. As a consequence, the smooth post-tunable parameter, i.e. the refractive index of the core n_{core}, becomes usable, which would benefit the experimental implementations of EPs in rolled-up tubular microcavities. Last but not least, rolled-up tubular microcavities are very long compared to the wavelength considered, which is opposite to the short microdisk microcavities. As we have mentioned above, the refractive index n in the two-dimensional Helmholtz equation (3) is not an effective one as presented in microdisk microcavities. Therefore, it has less wavelength dependency in rolled-up tubular microcavities, which improves the stability of parameters for pursuing EPs. Anyway, there arise new possibilities for the experimental realization of EPs in rolled-up tubular microcavity due to its subwavelength-thin wall, hollow core, and long length, which are, however, absent in microdisk microcavities.

Benefiting from these particularities in rolled-up tubular microcavities, EPs might be realized in the configuration of a microfluidic channel (μ-channel) structure, as shown in figure 5. Actually, rolled-up tubular microcavities have been experimentally demonstrated to be very suitable for optofludics due to their integrability into the μ-channels [16], compared with other optical microcavities supporting whispering gallery modes [38]. Therefore, the integration of rolled-up tubular microcavities with μ-channels would be an applicable solution for both the experimental realization of EPs and the label-free optofluidic detection using them. Under this experimental configuration, the spectral information of a rolled-up tubular microcavity as a subtle change in the refractive index n_{core} of liquid solution can be easily obtained by means of a μ-PL spectroscopy. Then, by monitoring the evolution of both resonant wavelength and Q factor as n_{core} varies for several degenerate mode pairs, one might find an EP according to the crossing and anti-crossing behaviors around it. Furthermore, one can perform label-free optofluidic detection using EPs.

5. Conclusion

We have observed the crossing and anti-crossing behaviors of nearly degenerate pairs of modes in rolled-up tubular microcavities by varying the overlap length between structural notches. We have pointed out that complex crossing and anti-crossing behaviors result from weak and strong couplings between the modes, based on a simple model of two-level open system with an effective coupling. EPs are the critical point where a transition from strong to weak coupling occurs, and are thus obtained in rolled-up tubular microcavities. Rolled-up microcavities with a single resonant mode approaching an EP have also been realized in parameter space expanded by two continuous variables. We have thus demonstrated EPs in rolled-up tubular microcavities without using near-field probes. Microcavities with EPs prepared in a rolled-up way could be mechanically stable and benefit to EP-based modern sensing applications. These findings add functionality to EP-based optical detection and show deeper physics in rolled-up tubular microcavities.

Acknowledgments

This work is supported by the Natural Science Foundation of China (No. 51322201), the Specialized Research Fund for the Doctoral Program of Higher Education (No. 20120071110025) and the Science and Technology Commission of Shanghai Municipality (No. 14JC1400200). One of the authors (SK) acknowledges financial support from the Research Chair Grant, the National Science and Technology Development Agency (NSTDA), Thailand. SK also thanks the Fundan Fellow Program, People's Republic of China.

References

[1] Heiss W D 2004 Exceptional points of non-Hermitian operators *J. Phys. A: Math. Theor.* **37** 2455
[2] Seyranian A P, Kirillov O N and Mailybaev A A 2005 Coupling of eigenvalues of complex matrices at diabolic and exceptional points *J. Phys. A: Math. Theor.* **38** 1723
[3] Heiss W D 2012 The physics of exceptional points *J. Phys. A: Math. Theor.* **45** 444016
[4] Ryu J-W, Son W-S, Hwang D-U, Lee S-Y and Kim S W 2015 Exceptional points in coupled dissipative dynamical systems *Phys. Rev.* E **91** 052910
[5] Dembowski C, Dietz B, Gräf H-D, Harney H L, Heine A, Heiss W D and Richter A 2004 Encircling an exceptional point *Phys. Rev.* E **69** 056216
[6] Gao T *et al* 2015 Observation of non-Hermitian degeneracies in a chaotic exciton-polariton billiard *Nature* **526** 554
[7] Cao H and Wiersig J 2015 Dielectric microcavities: model systems for wave chaos and non-Hermitian physics *Rev. Mod. Phys.* **87** 61–111
[8] Yin X and Zhang X 2013 Unidirectional light propagation at exceptional points *Nat. Mater.* **12** 175
[9] Gu Z, Zhang N, Lyu Q, Li M, Xiao S and Song Q 2016 Experimental demonstration of PT-symmetric stripe lasers *Laser Photonics Rev.* **10** 588

[10] Wiersig J 2014 Enhancing the sensitivity of frequency and energy splitting detection by using exceptional points: application to microcavity sensors for single-particle detection *Phys. Rev. Lett.* **112** 203901
[11] Wiersig J 2016 Sensors operating at exceptional points: General theory *Phys. Rev.* A **93** 033809
[12] Zhang N, Liu S, Wang K, Gu Z, Li M, Yi N, Xiao S and Song Q 2015 Single nanoparticle detection using far-field emission of photonic molecule around the exceptional point *Sci. Rep.* **5** 11912
[13] Zhu J, Özdemir S K, He L and Yang L 2010 Controlled manipulation of mode splitting in an optical microcavity by two Rayleigh scatterers *Opt. Express* **18** 23535
[14] Peng B, Özdemir S K, Liertzer M, Chen W, Kramer J, Yilmaz H, Wiersig J, Rotter S and Yang L 2016 Chiral modes and directional lasing at exceptional points *Proc. Nat. Acad. Sci. USA* **113** 6845
[15] Wang J, Zhan T, Huang G, Cui X, Hu X and Mei Y 2012 Tubular oxide microcavity with high-index-contrast walls: Mie scattering theory and 3D confinement of resonant modes *Opt. Express* **20** 18555–67
[16] Harazim S M, Bolaños Quiñones V A, Kiravittaya S, Sanchez S and Schmidt O G 2012 Lab-in-a-tube: on-chip integration of glass optofluidic ring resonators for label-free sensing applications *Lab Chip* **12** 2649
[17] Bernardi A, Kiravittaya S, Rastelli A, Songmuang R, Thurmer D J, Benyoucef M and Schmidt O G 2008 On-chip Si/SiOx microtube refractometer *Appl. Phys. Lett.* **93** 094106
[18] Huang G, Quiñones V A B, Ding F, Kiravittaya S, Mei Y and Schmidt O G 2010 Rolled-up optical microcavities with subwavelength wall thicknesses for enhanced liquid sensing applications *ACS Nano* **4** 3123
[19] Kipp T, Welsch H, Strelow C, Heyn C and Heitmann D 2006 Optical modes in semiconductor microtube ring resonators *Phys. Rev. Lett.* **96** 077403
[20] Songmuang R, Rastelli A, Mendach S and Schmidt O G 2007 SiO_x/Si radial superlattices and microtube optical ring resonators *Appl. Phys. Lett.* **90** 091905
[21] Strelow C, Rehberg H, Schultz C M, Welsch H, Heyn C, Heitmann D and Kipp T 2008 Optical microcavities formed by semiconductor microtubes using a bottlelike geometry *Phys. Rev. Lett.* **101** 127403
[22] Mei Y, Huang G, Solovev A A, Ureña E B, Mönch I, Ding F, Reindl T, Fu R K Y, Chu P K and Schmidt O G 2008 Versatile approach for integrative and functionalized tubes by strain engineering of nanomembranes on polymers *Adv. Mater.* **20** 4085
[23] Böttner S, Li S, Trommer J, Kiravittaya S and Schmidt O G 2012 Sharp whispering-gallery modes in rolled-up vertical SiO_2 microcavities with quality factors exceeding 5000 *Opt. Lett.* **37** 5136
[24] Quiñones V A B, Ma L, Li S, Jorgensen M R, Kiravittaya S and Schmidt O G 2012 Enhanced optical axial confinement in asymmetric microtube cavities rolled up from circular-shaped nanomembranes *Opt. Lett.* **37** 4284
[25] Ma L, Li S, Quiñones V A B, Yang L, Xi W, Jorgensen M R, Baunack S, Mei Y, Kiravittaya S and Schmidt O G 2013 Dynamic molecular processes detected by microtubular opto-chemical sensors self-assembled from prestrained nanomembranes *Adv. Mater.* **25** 2357
[26] Deng H, Haug H and Yamamoto Y 2010 Exciton-polariton Bose–Einstein condensation *Rev. Mod. Phys.* **82** 1489
[27] Böttner S, Li S, Jorgensen M R and Schmidt O G 2013 Vertically aligned rolled-up SiO_2 optical microcavities in add-drop configuration *Appl. Phys. Lett.* **102** 251119
[28] Böttner S, Li S, Jorgensen M R and Schmidt O G 2014 Polarization resolved spatial near-field mapping of optical modes in an on-chip rolled-up bottle microcavity *Appl. Phys. Lett.* **105** 121106
[29] Yin Y, Li S, Böttner S, Yuan F, Giudicatti S, Naz E S G, Ma L and Schmidt O G 2016 Localized surface plasmons selectively coupled to resonant light in tubular microcavities *Phys. Rev. Lett.* **116** 253904
[30] Wiersig J 2011 Structure of whispering-gallery modes in optical microdisks perturbed by nanoparticles *Phys. Rev.* A **84** 063828
[31] Strelow C, Schultz C M, Rehberg H, Sauer M, Welsch H, Stemmann A, Heyn C, Heitmann D and Kipp T 2012 Light confinement and mode splitting in rolled-up semiconductor microtube bottle resonators *Phys. Rev.* B **85** 155329
[32] Hosoda M and Shigaki T 2007 Degeneracy breaking of optical resonance modes in rolled-up spiral microtubes *Appl. Phys. Lett.* **90** 181107
[33] Li S, Ma L, Böttner S, Mei Y, Jorgensen M R, Kiravittaya S and Schmidt O G 2013 Angular position detection of single nanoparticles on rolled-up optical microcavities with lifted degeneracy *Phys. Rev.* A **88** 033833
[34] Fang Y, Li S and Mei Y 2016 Modulation of high quality factors in rolled-up microcavities *Phys. Rev.* A **94** 033804
[35] Song Q and Cao H 2010 Improving optical confinement in nanostructures via external mode coupling *Phys. Rev. Lett.* **105** 053902
[36] Lee S B, Yang J, Moon S, Lee S Y, Shim J B, Kim S W, Lee J H and An K 2009 Observation of an exceptional point in a chaotic optical microcavity *Phys. Rev. Lett.* **103** 134101
[37] Breuer H-P and Petruccione F 2002 *The Theory of Open Quantum Systems* (Oxford: Oxford University Press)
[38] Vahala K J 2003 Optical microcavities *Nature* **424** 839